Available online at www.sciencedirect.com

ScienceDirect

Mendeleev Commun., 2021, **31**, 30–32

Mendeleev Communications

Synthesis and characterization of benzobisthiazole based polymers as donor materials for organic solar cells

Petr M. Kuznetsov,[a] Ilya E. Kuznetsov,[a] Irina V. Klimovich,[a,b] Pavel A. Troshin[b,a] and Alexander V. Akkuratov*[a]

[a] *Institute for Problems of Chemical Physics, Russian Academy of Sciences, 142432 Chernogolovka, Moscow Region, Russian Federation. E-mail: akkuratow@yandex.ru*

[b] *Skolkovo Institute of Science and Technology, 143025 Moscow, Russian Federation*

DOI: 10.1016/j.mencom.2021.01.008

Two conjugated polymers with (X-DADAD)$_n$ backbone and 2,6- or 4,8-linked benzobisthiazole (BBT) moieties were designed, synthesized and characterized as absorber materials in thin-film organic solar cells (OSCs). The 2,6-BBT polymer (P1) delivered enhanced short circuit densities and power conversion efficiencies in OSCs compared to devices based on 4,8-BBT polymer P2. Improved photovoltaic performance is related to the optimal morphology of P1/PC$_{71}$BM blend films and higher and more balanced charge carrier mobilities.

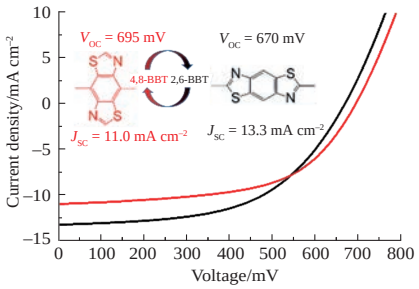

Keywords: conjugated polymers, benzobisthiazole, fullerene acceptor, doctor-blade coating, organic solar cells.

Organic solar cells (OSCs) have attracted considerable attention due to their advantages over traditional silicon solar cells, such as flexibility, light weight, and simple and low-cost fabrication using roll-to-roll printing and coating technologies.[1–3] Furthermore, the outstanding power conversion efficiencies (PCEs) of ~18%[4] make OSCs attractive for industry-scale production and commercialization.[5–7] The performance of OSCs has been improved due to the development of donor conjugated polymers and fullerene derivatives or non-fullerene acceptor compounds. The most well-performing electron donor polymers are designed according to a widely used push–pull strategy involving the alternation of electron-donor and electron-acceptor building blocks in the backbone in order to modulate the electronic and optical properties of conjugated polymers and control their charge-transport characteristics and self-ordering in a solid state.

Here, we report the synthesis and characterization of two (X-DADAD)$_n$-type conjugated polymers comprising 2,6- and 4,8-linked benzobisthiazole (BBT) blocks (X fragment) in combination with a thiophene (D) and benzothiadiazole (A) DADAD framework. Recently, we showed that (X-DADAD)$_n$ polymers and small molecules are promising materials for the fabrication of efficient and stable OSCs and larger-area modules.[8–11] The introduction of a BBT building block can induce intramolecular noncovalent interactions, which facilitate the planarization of polymer chains and their efficient π-π stacking in thin films[12] thus improving charge carrier mobilities and, hence, the overall photovoltaic performance of BBT-based polymers in OSCs.

Scheme 1 shows the synthesis of conjugated polymers **P1** and **P2**. The palladium-catalyzed Stille polycondensation reaction between 2,5-bis(7-(3'-(2-hexyldecyl)-5'-(trimethylstannyl)-

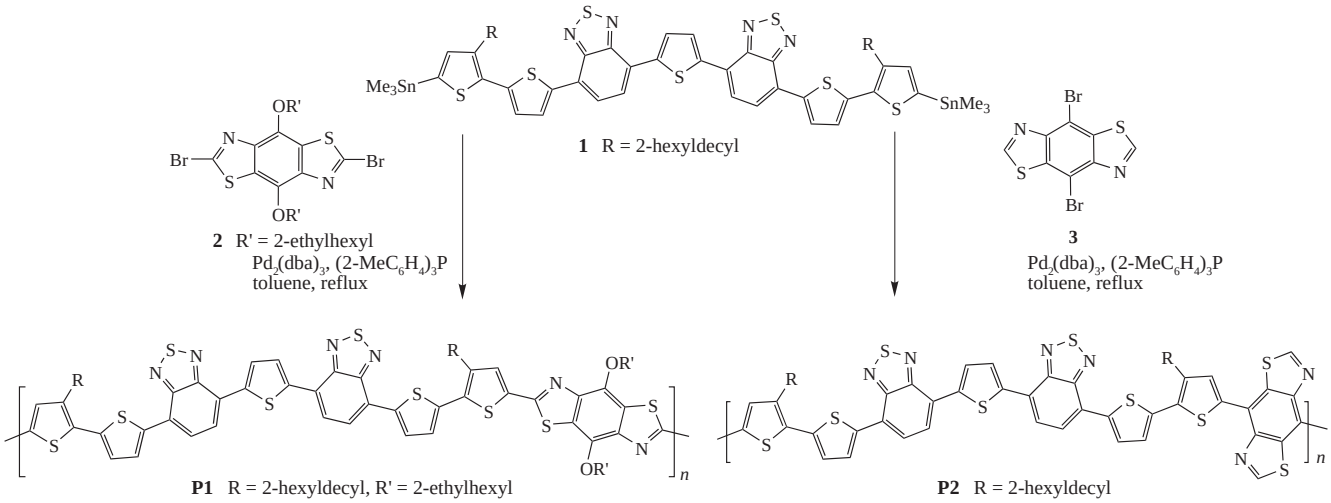

Scheme 1 Synthesis of conjugated polymers **P1** and **P2**.

Table 1 Physicochemical, optical and electrochemical properties of polymers **P1** and **P2**.

Polymer	M_w/[a]kDa	M_w/M_n[b]	$E^{ox.}_{onset}$/[c]V *vs.* Fc^+/Fc	HOMO/[d]eV	LUMO/[e]eV	$\lambda^{sol}_{max}/\lambda^{film}_{max}/\lambda^{film}_{edge}$/[f]nm	E_g^{opt}/[g]eV
P1	58	1.7	0.40	–5.50	–3.84	538/629/751	1.66
P2	62	1.5	0.50	–5.60	–4.02	556/650/789	1.58

[a] Weight-average molecular weight. [b] Polydispersity index. [c] Oxidation potential. [d] HOMO energy was estimated by CV measurements. [e] LUMO energy was estimated as E_g^{opt} + HOMO. [f] Absorption maxima of polymers in solution/thin film/absorption edge of thin film spectra. [g] Optical energy bandgap.

[2,2'-bithiophen]-5-yl)benzo[*c*][1,2,5]thiadiazol-4-yl)-thiophene[9] **1** and 2,6-dibromo-4,8-bis[(2-ethylhexyl)oxy]-benzo[1,2-d:4,5-d']bis(thiazole)[13] **2** or 4,8-dibromobenzo-[1,2-d:4,5-d']bis(thiazole)[14,15] **3** afforded polymers **P1** and **P2**, respectively, with isolated yields of 54–65% (see Online Supplementary Materials).

Molecular weight characteristics of polymers were analyzed by gel-permeation chromatography as described previously[16] using chlorobenzene as an eluent at 50 °C. The weight-average molecular weights were estimated as 58 and 62 kDa for **P1** and **P2**, respectively (Table 1, Figure S1). The polymers are soluble in toluene, chlorobenzene, and 1,2-dichlorobenzene.

The polymers exhibited similar optical properties in dilute 1,2-dichlorobenzene solutions with absorption maxima at 538 and 556 nm for **P1** and **P2**, respectively [Figure 1(*a*)]. The absorption maxima were spectacularly red-shifted by 91–94 nm in the spectra of thin films of **P1** and **P2** due to a strong self-organization of the polymers enabling efficient intermolecular contacts in a solid state. The long-wavelength absorption edge (λ^{film}_{edge}) of 2,6-BBT-based polymer **P1** at 751 nm corresponds to an optical bandgap (E_g) of 1.66 eV, while 4,8-BBT-containing polymer **P2** showed lower bandgap of 1.58 eV. The thin-film absorption spectra of polymer **P1** had intense absorption peaks in the short-wavelength region (~300–550 nm) caused by strong π–π interactions between the polymer chains in a solid state. These optical properties of the material can contribute to the generation of higher photocurrents in OSCs.

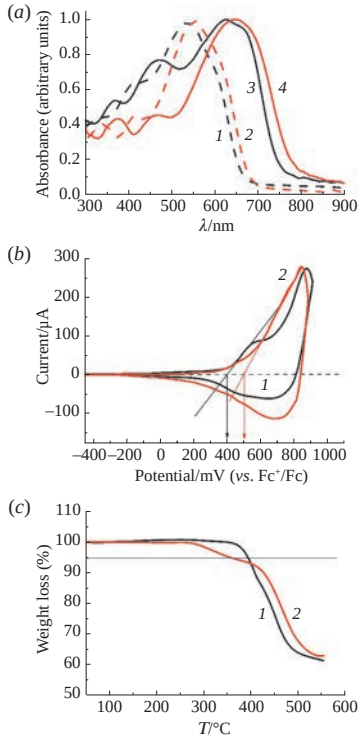

Figure 1 *(a)* Absorption spectra of polymers (*1*) **P1** and (*2*) **P2** in 1,2-dichlorobenzene and (*3*) **P1** and (*4*) **P2** in films; *(b)* the cyclic voltammograms of thin polymer films of (*1*) **P1** and (*2*) **P2** deposited on a glassy carbon disk electrode in a 0.1 M Bu_4NPF_6 solution in acetonitrile as supporting electrolyte (scan rate, 50 mV s^{-1}); *(c)* TGA curves of polymers (*1*) **P1** and (*2*) **P2**.

Cyclic voltammetry (CV) was used to estimate the highest occupied molecular orbital (HOMO) energies of the polymers [Figure 1(*b*)].

The oxidation potentials were estimated as 0.4 V for polymer **P1** and 0.5 V for polymer **P2** *vs.* a Fc^+/Fc redox couple with an absolute energy of –5.10 eV *vs.* a vacuum level. The HOMO energies were calculated from the equation $E_{HOMO} = -e(E^{ox.}_{onset}+5.1)$ (eV).[17] Table 1 indicates that the HOMO energy level of 4,8-BBT-based polymer **P1** (–5.50 eV) lies 0.1 eV higher than that of 2,6-BBT-based analogue **P2** (–5.60 eV). This can be due to electron-donating alkoxy side chains incorporated in the structure of polymer **P1**, as described previously.[18]

The thermal properties of polymers were studied by thermal gravimetry [Figure 1(*c*)]. The polymers showed high thermal stability with decomposition temperatures (T_d, 5%) of 390 and 355 °C for **P1** and **P2**, respectively. Differential scanning calorimetry (DSC) analysis revealed no phase transitions in the polymers upon heating and cooling in a nitrogen atmosphere (Figure S2, Online Supplementary Materials).

The polymers were investigated as electron donor materials in OSCs with the standard configuration: glass/ITO/PEDOT:PSS(30 nm)/active layer/Mg (50 nm)/Al (100 nm). The fullerene derivative $PC_{71}BM$ was used as an acceptor component.[19] The active layers were deposited from 1,2-dichlorobenzene using a doctor-blade method, which is compatible with roll-to-roll processing techniques. The **P1**/$PC_{71}BM$ blends were prepared with weight ratio of 1–1.5 between the components, whereas the optimal film thickness was ~120 nm. The optimum composition of the **P2**/$PC_{71}BM$ system was 1 : 2 (by weight), and the optimal film thickness was ~130 nm. Thermal annealing at 95 °C for 10 min was optimal for both **P1**/$PC_{71}BM$ and **P2**/$PC_{71}BM$ blends. Figure 2 shows the *J*–*V* curves and EQE spectra of the optimized devices, and Table 2 summarizes their parameters.

The **P1**-based OSCs delivered a PCE of 4.9% with V_{OC} of 670 mV, J_{SC} of 13.3 mA cm^{-2} and FF of 55%. At the same time, polymer **P2** provided a slightly lower PCE of 4.4% with V_{OC} of 695 mV, J_{SC} of 13.3 mA cm^{-2} and FF of 57%.

The higher open circuit voltages of OSCs based on polymer **P2** can be attributed to its low-lying HOMO energy level.[20] The short-circuit current densities obtained from *J*–*V* measurements are consistent with the values of J_{SC} estimated from EQE spectra by their integration over true solar AM1.5G solar spectrum [Figure 2(*b*), Table 2].

In order to gain a deeper insight into the origins of different photovoltaic performances of polymers **P1** and **P2**, we assessed the charge-transport characteristics of photoactive polymer–fullerene blends. The hole and electron mobilities of the blends prepared under optimal conditions were measured using the SCLC method[21] for hole-only devices with the structure of ITO/PEDOT:PSS (60 nm)/blend/MoO_3 (22 nm)/Ag (120 nm) and electron-only devices with the structure of ITO/Yb (15 nm)/blend/Sm (100 nm). Table 2 summarizes the resulting values of μ_h and μ_e, and the corresponding $J^{1/2}$–*V* plots are given in Figure S3 (Online Supplementary Materials). The charge carrier mobilities of the **P1**/$PC_{71}BM$ blends are higher and more balanced (μ_h/μ_e) compared to those in the **P2**/$PC_{71}BM$ system. Thus, the increased J_{SC} obtained for **P1**-based OSCs can be attributed to improved charge carrier mobilities and, hence, reduced recombination losses.

Table 2 Characteristics of organic solar cells based on polymers **P1** and **P2** blended with $PC_{71}BM$.

Polymer	V_{OC}/[a]mV	J_{SC}/J_{SC}^{EQE}/[b]mA cm^{-2}	FF (%) [c]	η (%) [d]	μ_h/[e]cm^2 V^{-1} s^{-1}	μ_e/[f]cm^{2}V^{-1}s^{-1}	μ_h/μ_e[g]
P1	670±6	13.3±0.3/13.5	55±2.0	4.9±0.3	6.4×10^{-5}	6.1×10^{-5}	1.04
P2	695±8	11.0±0.3/11.1	57±1.6	4.4±0.2	3.4×10^{-5}	4.7×10^{-5}	0.72

[a] Open-circuit voltages. [b] Short-circuit currents from *J*–V measurements/from EQE spectra. [c] Fill factors. [d] Power conversion efficiency, average characteristics for a batch of nine devices. [e] Hole mobilities of blend films. [f] Electron mobilities of blend films. [g] The ratio of hole and electron mobilities.

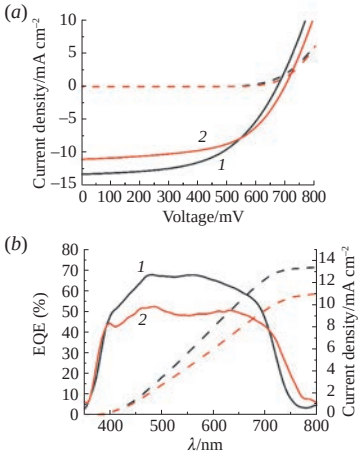

Figure 2 *(a) J–V* curves and *(b)* EQE spectra of organic solar cells based on polymers (*1*) **P1** and (*2*) **P2**.

We studied the morphology of the optimized composite fullerene–polymer blends using atomic force microscopy (AFM) (Figure 3).

The average cluster sizes were estimated at 10 and 31 nm for the **P1**/$PC_{71}BM$ and **P2**/$PC_{71}BM$ blend films, respectively, which are comparable with typical exciton diffusion lengths in organic semiconductors (10–25 nm).[22] However, the **P2**-based films are rougher with a root-mean-square (RMS) roughness of 1.28 nm, as compared to the **P1**/$PC_{71}BM$ blends with a noticeably lower RMS of 0.89 nm. The increased RMS values for composite films suggest insufficient miscibility of polymer **P2** with a $PC_{71}BM$ acceptor, which can result in enhanced recombination of charge carriers and hence decreased short circuit currents of the corresponding solar cells.

We believe that the performance of the designed polymers in OSCs can be improved by their use in combination with promising non-fullerene acceptors or incorporation in ternary systems.[23,24]

Thus, we synthesized and characterized two conjugated polymers comprising 2,6-BBT (**P1**) and 4,8-BBT (**P2**) units to be used in organic solar cells as electron donor materials with the acceptor fullerene derivative $PC_{71}BM$. Polymer **P1** provided higher short circuit current densities in OSCs compared to polymer **P2**, which is associated with superior charge transport characteristics and a more balanced morphology of **P1**/ $PC_{71}BM$ blend films.

This work was supported by the Russian Foundation for Basic Research (project no. 18-33-20025) and the Ministry of Science and Higher Education of the Russian Federation [project no. AAA-A19-119071190044-3 (0089-2019-0010)].

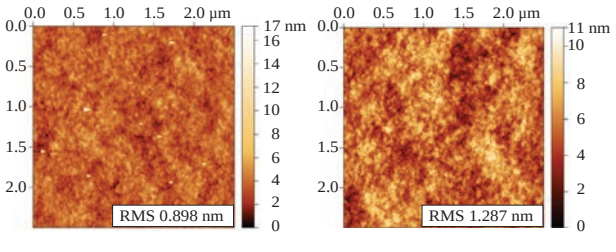

Figure 3 AFM images for optimized **P1**/$PC_{71}BM$ and **P2**/$PC_{71}BM$ blends.

Online Supplementary Materials

Supplementary data associated with this article can be found in the online version at doi: 10.1016/j.mencom.2021.01.008.

References

1 S. Ganesan, S. Mehta and D. Gupta, *Opto-Electron. Rev.*, 2019, **27**, 298.
2 A. S. Gertsen, M. F. Castro, R. R. Søndergaard and J. W. Andreasen, *Flex. Print. Electron.*, 2020, **5**, 014004.
3 R. Søndergaard, M. Hösel, D. Angmo, T. T. Larsen-Olsen and F. C. Krebs, *Mater. Today*, 2012, **15**, 36.
4 Q. Liu, Y. Jiang, K. Jin, J. Qin, J. Xu, W. Li, J. Xiong, J. Liu, Z. Xiao, K. Sun, S. Yang, X. Zhang and L. Ding, *Sci. Bull.*, 2020, **65**, 272.
5 M. J. Griffith, S. Cottam, J. Stamenkovic, J. A. Posar and M. Petasecca, *Front. Phys.*, 2020, **8**, doi.org/10.3389/fphy.2020.00022.
6 M. J. Griffith, N. P. Holmes, D. C. Elkington, S. Cottam, J. Stamenkovic, A. L. D. Kilcoyne and T. R. Andersen, *Nanotechnology*, 2019, **31**, 092002.
7 E. Ravishankar, R. E. Booth, C. Saravitz, H. Sederoff, H. W. Ade and B. T. O'Connor, *Joule*, 2020, **4**, 490.
8 A. V. Akkuratov, S. L. Nikitenko, A. S. Kozlov, P. M. Kuznetsov, I. V. Martynov, N. V. Tukachev, A. Zhugayevych, I. Visoly-Fisher, E. A. Katz and P. A. Troshin, *Sol. Energy*, 2020, **198**, 605.
9 A. V. Akkuratov, I. E. Kuznetsov, I. V. Martynov, D. K. Sagdullina, P. M. Kuznetsov, L. Ciammaruchi, F. A. Prudnov, M. V. Klyuev, E. A. Katz and P. A. Troshin, *Polymer*, 2019, **183**, 121849.
10 A. V. Akkuratov, D. K. Susarova, O. V. Kozlov, A. V. Chernyak, Y. L. Moskvin, L. A. Frolova, M. S. Pshenichnikov and P. A. Troshin, *Macromolecules*, 2015, **48**, 2013.
11 (*a*) P. M. Kuznetsov, S. L. Nikitenko, I. E. Kuznetsov, P. I. Proshin, D. V. Revina, P. A. Troshin and A. V. Akkuratov, *Tetrahedron Lett.*, 2020, **61**, 152037; (*b*) I. E. Kuznetsov, P. M. Kuznetsov, A. V. Maskaev, A. V. Akkuratov and P. A. Troshin, *Mendeleev Commun.*, 2020, **30**, 683.
12 Y.-H. So, S. J. Martin, B. Bell, C. D. Pfeiffer, R. M. Van Effen, B. L. Romain and S. M. Lefkowitz, *Macromolecules*, 2003, **36**, 4699.
13 T. L. D. Tam and T. T. Lin, *Macromolecules*, 2016, **49**, 1648.
14 J. F. Wolfe, B. H. Loo and F. E. Arnold, *Macromolecules*, 1981, **14**, 915.
15 G. Conboy, R. G. D. Taylor, N. J. Findlay, A. L. Kanibolotsky, A. R. Inigo, S. S. Ghosh, B. Ebenhoch, L. K. Jagadamma, G. K. V. V. Thalluri, M. T. Sajjad, I. D. W. Samuel and P. J. Skabara, *J. Mater. Chem. C*, 2017, **5**, 11927.
16 A. V. Akkuratov, F. A. Prudnov, L. N. Inasaridze and P. A. Troshin, *Tetrahedron Lett.*, 2017, **58**, 97.
17 C. M. Cardona, W. Li, A. E. Kaifer, D. Stockdale and G. C. Bazan, *Adv. Mater.*, 2011, **23**, 2367.
18 X. Guo, Q. Liao, E. F. Manley, Z. Wu, Y. Wang, W. Wang, T. Yang, Y.-E. Shin, X. Cheng, Y. Liang, L. X. Chen, K.-J. Baeg, T. J. Marks and X. Guo, *Chem. Mater.*, 2016, **28**, 2449.
19 M. M. Wienk, J. M. Kroon, W. J. H. Verhees, J. Knol, J. C. Hummelen, P. A. van Hal and R. A. J. Janssen, *Angew. Chem., Int. Ed.*, 2003, **115**, 3493.
20 C. J. Brabec, A. Cravino, D. Meissner, N. S. Sariciftci, T. Fromherz, M. T. Rispens, L. Sanchez and J. C. Hummelen, *Adv. Funct. Mater.*, 2001, **11**, 374.
21 Y. Xin, G. Zeng, J. Ouyang, X. Zhao and X. Yang, *J. Mater. Chem. C*, 2019, **7**, 9513.
22 Y. Zhang, M. T. Sajjad, O. Blaszczyk, A. J. Parnell, A. Ruseckas, L. A. Serrano, G. Cooke and I. D. W. Samuel, *Chem. Mater.*, 2019, **31**, 6548.
23 N. Gasparini, A. Salleo, I. McCulloch and D. Baran, *Nat. Rev. Mater.*, 2019, **4**, 229.
24 P. Bi and X. Hao, *Sol. RRL*, 2019, **3**, 1800263.

Received: 21st September 2020; Com. 20/6317